Kirchhoff approximation for diffusive waves

Jorge Ripoll*
Institute for Electronic Structure and Laser, Foundation for Research and Technology-Hellas, P.O. Box 1527, 71110 Heraklion, Crete, Greece

Vasilis Ntziachristos
Center For Molecular Imaging Research, Massachusetts General Hospital & Harvard Medical School, Building 149, 13th Street 5406, Charlestown, Massachusetts 02129-2060

Remi Carminati
Laboratoire d'Energetique Moleculaire et Macroscopique, Combustion, Ecole Centrale Paris, Centre National de la Recherche, Scientifique, 92295 Chatenay-Malabry Cedex, France

Manuel Nieto-Vesperinas
Instituto de Ciencia de Materiales, Consejo Superior de Investigaciones Cientificas, Campus de Cantoblanco, 28049 Madrid, Spain
(Received 28 May 2001; revised manuscript received 9 August 2001; published 26 October 2001)

Quantitative measurements of diffuse media, in spectroscopic or imaging mode, rely on the generation of appropriate forward solutions, independently of the inversion scheme employed. For complex boundaries, the use of numerical methods is generally preferred due to implementation simplicity, but usually results in great computational needs, especially in three dimensions. Analytical expressions are available, but are limited to simple geometries such as a diffusive slab, a sphere or a cylinder. An analytical approximation, the Kirchhoff approximation, also called the tangent-plane method is presented for the case of diffuse light. Using this approximation, analytical solutions of the diffusion equation for arbitrary boundaries and volumes can be derived. Also, computation time is minimized since no matrix inversion is involved. The accuracy of this approximation is evaluated on comparison with results from a rigorous numerical technique calculated for an arbitrary geometry. Performance of the approximation as a function of the optical properties and the size of the medium is examined and it is demonstrated that the computation time of the direct scattering model is reduced at least by two orders of magnitude.

DOI: 10.1103/PhysRevE.64.051917 PACS number(s): 87.10.+e, 42.25.Fx, 42.30.Wb, 42.62.Be

I. INTRODUCTION

The study of light transport through highly scattering media, such as tissue, has been the focus of recent research geared towards medical diagnostics [1–9]. This has been motivated by the fact that light offers unique contrast mechanisms while probing structural and functional tissue characteristics. Furthermore, the associated technology employs nonionizing radiation and is generally low cost. Imaging through tissues using light in the near infrared (NIR) spectral region offers penetration capability of several centimeters due to the low absorption by tissue in the 700–850 nm spectral region. Lately, rigorous mathematical modeling of light propagation in tissue (see Ref. [10] for a review), combined with technological advancements in photon sources and detection techniques, has made possible the application of tomographic principles [11] for NIR three-dimensional imaging of the internal optical contrast of tissue, using a technique generally termed diffuse optical tomography (DOT) [5–22].

At the moment, powerful numerical methods are available for accurately solving the direct scattering problem [17,18,23] for arbitrary geometries, but these methods are computationally costly. A fast method that can be applied to arbitrary geometries is needed for real time diagnostics. A good candidate is the Kirchhoff approximation (KA), also called the tangent-plane method [25,26]. This approximation is a linear method that does not involve matrix inversion while solving the forward problem. The KA can be used to generate the sensitivity functions (or weights) of the system, so that inversion schemes such as algebraic reconstruction techniques (ART) [11], amongst others, may be applied. Also, since it generates the complete Green function for any three-dimensional (3D) geometry, it is possible to apply it to improve the already existing reconstruction methods that use the Born or Rytov approximations [6–9,11–15].

The KA is a well-known approximation in physical optics that has been under study for over 30 years, and, in particular, extensively employed in studies of scattering from rough surfaces (see Ref. [26] and references therein). In these cases, the validity of the KA has been usually studied versus the angle of incidence. We here study the performance of the KA for a point source in an arbitrary diffusive medium in order to demonstrate the potential of the KA in diffuse optical tomography. We would like to state that a more rigorous study of the limits of validity of the KA would imply calculating the error for each frequency component of the incident wave, but this is out of the scope of the present paper.

In this work, we present the theory of the Kirchhoff ap-

*Email address: jripoll@iesl.forth.gr

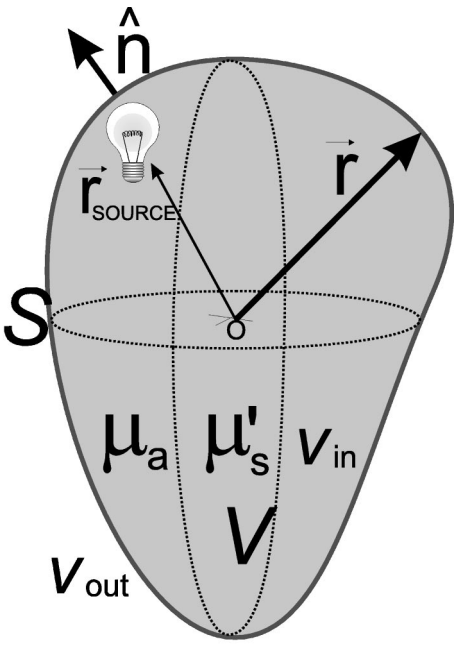

FIG. 1. Scattering geometry.

proximation in the diffusion equation context, and study its limits of validity. In Sec. II we present the exact expression for the Green function for arbitrary diffusive volumes. In Sec. III we introduce the KA specifics and derive the expression for the approximate Green function for an arbitrary geometry from the exact expression. The limits of validity of the KA are studied in Sec. IV as a function of the medium's size and optical properties. We demonstrate that these limits are independent of the geometry and depend mainly on the size of the system in diffusion length units. KA is applied to an arbitrary geometry, and compared with results obtained when employing an accurate numerical method and the infinite homogeneous Green function. We investigate the accuracy of the KA and compare the computational times of both methods, demonstrating that the KA is more than two orders of magnitude faster than accurate numerical methods and, therefore, could be a very useful tool for DOT. Finally, we conclude in Sec. V.

II. THEORY: EXACT EXPRESSION FOR THE GREEN FUNCTION

Let us consider the geometry shown in Fig. 1, consisting of a diffusive volume V bounded by surface S, which separates it from an outer nondiffusive medium of refractive index ν_{out}. This diffusive medium is characterized by its absorption coefficient μ_a, the diffusion coefficient $D=\frac{1}{3}(\mu_s'+\alpha\mu_a)$ (where μ_s' is the reduced scattering coefficient), and the refractive index ν_{in}. In the expression for D, the factor α does not have a closed-form expression and has values that range from $\alpha=0$ to $\alpha=1$ depending on the approximation used (see Ref. [24] and references therein for more insight on the subject). Even so, since we have not found significant differences in the results presented here when introducing the dependence of D on absorption, we shall use $\alpha=0$ for simplicity. If the incident light impinging on the medium is modulated at a frequency ω, the average intensity $U(\mathbf{r},t)=U(\mathbf{r})\exp[-i\omega t]$ detected at $\mathbf{r}$ represents a diffuse photon density wave (DPDW) [1] and obeys the Helmholtz equation with a wave number $\kappa=(-\mu_a/D+i\omega\nu/cD)^{1/2}$, where c is the speed of light in vacuum, and ν is the refractive index of the medium. In an infinite homogeneous medium, the Green function g satisfies

$$\nabla^2 g(\kappa|\mathbf{r}_s-\mathbf{r}_d|)+\kappa^2 g(\kappa|\mathbf{r}_s-\mathbf{r}_d|)=-4\pi\delta(\mathbf{r}_s-\mathbf{r}_d), \quad (1)$$

where $\mathbf{r}_s$ and $\mathbf{r}_d$ represent the source and detector points, respectively. In 3D it is well known to be

$$g(\kappa|\mathbf{r}_s-\mathbf{r}_d|)=\frac{\exp[i\kappa|\mathbf{r}_s-\mathbf{r}_d|]}{|\mathbf{r}_s-\mathbf{r}_d|}. \quad (2)$$

In terms of the *complete* Green function $G(\mathbf{r}_s,\mathbf{r}_d)$ that corresponds to the full geometry in Fig. 1 with boundaries, the expression of the average intensity at a point $\mathbf{r}_d$ inside the medium is

$$U(\mathbf{r}_d)=\frac{1}{4\pi}\int_\nu \frac{S(\mathbf{r}')}{D}G(\mathbf{r}',\mathbf{r}_d)d\mathbf{r}', \quad \mathbf{r}_d\in V, \quad (3)$$

where $S(\mathbf{r}')$ represents the source distribution and V is the volume occupied by the diffusive medium. Of course, for a source in infinite space $G(\mathbf{r}_s,\mathbf{r}_d)=g(\kappa|\mathbf{r}_s-\mathbf{r}_d|)$.

The complete Green function inside the diffusive medium can be expressed in terms of its surface integral by means of Green's Theorem (see Refs. [23, 27] for a detailed derivation) as

$$G(\mathbf{r}_s,\mathbf{r}_d)=g(\kappa|\mathbf{r}_s-\mathbf{r}_d|)-\frac{1}{4\pi}\int_s\Bigg[G(\mathbf{r}_s,\mathbf{r}')\frac{\partial g(\kappa|\mathbf{r}'-\mathbf{r}_d|)}{\partial n'} - g(\kappa|\mathbf{r}'-\mathbf{r}_d|)\frac{\partial G(\mathbf{r}_s,\mathbf{r}')}{\partial \mathbf{n}'}\Bigg]dS', \quad (4)$$

where $\mathbf{n}'$ is the surface unit outward normal pointing into the nondiffusive medium (see Fig. 1), and $\partial/\partial\mathbf{n}'=\mathbf{n}'\cdot\nabla_{r'}$. The boundary condition between the diffusive and nondiffusive medium in the diffusion approximation is obtained by assuming that all the flux traversing the interface is outwards into the nondiffusive medium (see Ref. [28] for a detailed derivation). This is always true as long as no sources are located outside the diffusive medium. In terms of the Green function this boundary condition is expressed as [28–30]

$$G(\mathbf{r}_s,\mathbf{r}')|_s=-C_{\text{nd}}D\frac{\partial G(\mathbf{r}_s,\mathbf{r}')}{\partial\mathbf{n}'}\Bigg|_S, \quad \mathbf{r}'\in S, \quad (5)$$

where the coefficient C_{nd} takes into account the refractive index mismatch between both media [28]. In the case of index matched media, i.e., $\nu_{\text{out}}=\nu_{\text{in}}$, $C_{\text{nd}}=2$. Introducing Eq. (5) into Eq. (4), we obtain

$$G(\mathbf{r}_s,\mathbf{r}_d)=g(\kappa|\mathbf{r}_s-\mathbf{r}_d|)+\frac{1}{4\pi}\int_S\Big[C_{\mathrm{nd}}D\frac{\partial g(\kappa|\mathbf{r}'-\mathbf{r}_d)}{\partial\mathbf{n}'}+g(\kappa|\mathbf{r}'-\mathbf{r}_d|)\Big]\frac{\partial G(\mathbf{r}_s,\mathbf{r}')}{\partial\mathbf{n}'}dS'. \quad (6)$$

A rigorous solution to $G(\mathbf{r}_s,\mathbf{r}_d)$ in Eq. (6) is found by determining the boundary value $\partial G/\partial\mathbf{n}'$ by discretizing the surface S into a number of surface elements and inverting the resulting matrix (see Ref. [23] and references therein). Similarly to Ref. [23], Eq. (6) makes an indirect use of the extinction theorem in order to solve the system; hereon we will refer to this method as the *extinction theorem* (ET) method. The ET method gives a rigorous numerical solution to the forward problem, but is time consuming since it involves matrix inversion, and, therefore, is also limited to surfaces that can be segmented to a moderate number of discretisation points. For example, solving for more than 5000 surface points is generally excessive while considering the inverse problem, requiring about 1 h for one forward calculation on a Pentium III running at 650 MHz with 256 Mb memory. Even so, it must be understood that the computation times considered in this paper correspond to Eq. (6), which has only one unknown variable. In the case of a diffusive volume within a diffusive medium, the existence of two unknown variables (the average intensity and its derivative) increases the number of unknown variables by a factor of two. Hence, assuming that in order for the ET to give accurate results, the minimum distance between two discretization points must be in the order of the transport mean free path $l_{\mathrm{tr}}=1/\mu_s'$, the ET method would become inappropriate to solve the inverse problem for diffusive/nondiffusive surface areas in the order of 50 cm^2, or 25 cm^2 in the case of diffusive/diffusive profiles. This fact limits the applicability of exact methods in large geometries, such as the adult head. Anyhow, the use of exact methods such as the ET is fundamental in order to validate approximate methods (see Sec. 5 of Ref. [23], where a brief discussion of the need for exact methods in optical tomography is presented). Conversely, the computing time required is practically independent of the number of detector points since Eq. (6) provides for a direct solution of detector readings along the boundary simultaneously. This is general for all surface-value dependent methods.

III. THE KIRCHHOFF APPROXIMATION

When many forward solution calculations are required, such as in most tomographic schemes (except those reported in Ref. [16]), an approximation to Eq. (6) that can handle *arbitrary* 3D geometries in a linear fashion is needed, to reduce computing time and memory requirements. One such approximation is the KA, also known as the physical-optics or the tangent-plane method [25], which is well known and used in both optics and acoustics. This approximation assumes that the surface is replaced at each point by its tangent plane. This means that the value of the total intensity U at any point $\mathbf{r}_p$ of the surface S is given by the sum of the incident field $U^{(\mathrm{inc})}$ and the wave reflected from the *local plane* defined by the surface normal $\mathbf{n}(\mathbf{r}_p)$ at that surface point. In terms of the Green function this is expressed as

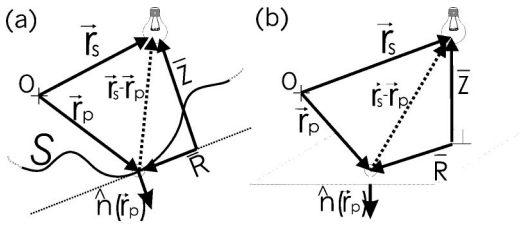

FIG. 2. (a) Detail of the local tangent plane used in the KA. (b) Representation in the coordinates of the tangent plane.

$$G^{\mathrm{KA}}(\mathbf{r}_s,\mathbf{r}_p)=g(\kappa|\mathbf{r}_s-\mathbf{r}_p|)*[1+R_{\mathrm{ND}}(\mathbf{r}_p)], \quad (7)$$

where $*$ denotes convolution, and R_{ND} is the reflection coefficient for diffusive waves in real space, which in Fourier space has the expression for each plane wave component of g [31],

$$R_{\mathrm{ND}}(\mathbf{K})=\frac{iC_{\mathrm{nd}}D\sqrt{\kappa^2-\mathbf{K}^2}+1}{iC_{\mathrm{nd}}D\sqrt{\kappa^2+\mathbf{K}^2}-1}. \quad (8)$$

In a similar manner, the gradient of the Green function is

$$\frac{\partial G^{\mathrm{KA}}(\mathbf{r}_s,\mathbf{r}_p)}{\partial\mathbf{n}_p}=\frac{\partial g(k|\mathbf{r}_s-\mathbf{r}_p|)}{\partial\mathbf{n}_p}*[1-R_{\mathrm{ND}}(\mathbf{r}_p)], \quad (9)$$

the minus sign takes into consideration the different propagation directions of the incident and reflected wave with respect to the local plane. Equations (7) and (9) are directly expressed in Fourier space as

$$G^{\mathrm{KA}}(\mathbf{r}_s,\mathbf{r}_p)=\int_{-\infty}^{+\infty}[1+R_{\mathrm{ND}}(\mathbf{K})]\tilde{g}(\mathbf{K},\bar{Z})\exp[i\mathbf{K}\cdot\bar{\mathbf{R}}]d\mathbf{K},$$

$$\frac{\partial G^{\mathrm{KA}}(\mathbf{r}_s,\mathbf{r}_p)}{\partial\hat{\mathbf{n}}_p}=\int_{-\infty}^{+\infty}[1-R_{\mathrm{ND}}(\mathbf{K})]\frac{\partial\tilde{g}(\mathbf{K},\bar{Z})}{\partial\bar{Z}}\exp[i\mathbf{K}\cdot\bar{\mathbf{R}}]d\mathbf{K}. \quad (10)$$

In order to numerically perform the Fourier transforms in Eq. (10), a typical number of values for $\mathbf{K}$ is 512 for each dimension, with $|d\mathbf{K}|\sim 0.123\ \mathrm{cm}^{-1}$, which corresponds to a spatial discretization value of $|d\mathbf{R}|=0.1$ cm. The need for a low number of $\mathbf{K}$ values is due to the fact that DPDW's are highly damped and do not contain high spatial frequencies. 256 values for $\mathbf{K}$ were also tested, finding differences smaller than 1%. In all cases presented in this work 512 $\mathbf{K}$ values were employed. In Eq. (10) $(\bar{\mathbf{R}},\bar{Z})$ are the coordinates of $|\mathbf{r}_s-\mathbf{r}_p|$ with respect to the plane defined by $\mathbf{n}(\mathbf{r}_p)$ as shown in Fig. 2, namely,

$$\bar{Z}=(\mathbf{r}_s-\mathbf{r}_p)\cdot[-\hat{\mathbf{n}}(\mathbf{r}_p)],$$
$$\bar{\mathbf{R}}=\bar{Z}-(\mathbf{r}_s-\mathbf{r}_p). \quad (11)$$

In Eq. (10) the Fourier transform $\tilde{g}(\mathbf{K},z)$ of the 3D homogeneous Green function $g(\kappa|\mathbf{r}_s-\mathbf{r}_p|)$ is given by [20,21,31,32]

$$\tilde{g}(\mathbf{K},\overline{Z}) = \frac{i}{2\pi}\frac{\exp[i\sqrt{\kappa^2-\mathbf{K}^2}|\overline{Z}|]}{\sqrt{\kappa^2-\mathbf{K}^2}},$$

$$\frac{\partial\tilde{g}(\mathbf{K},\overline{Z})}{\partial\overline{Z}} = \frac{1}{2\pi}\exp[i\sqrt{\kappa^2-\mathbf{K}^2}|\overline{Z}|]. \tag{12}$$

Therefore, if we discretise the surface S in Eq. (6) into N area elements ΔS, we can write the complete Green function given by Eq. (6) inside the volume V in terms of the KA as

$$G^{\mathrm{KA}}(\mathbf{r}_s,\mathbf{r}_d) = g(\kappa|\mathbf{r}_s-\mathbf{r}_d|) + \frac{\Delta S}{4\pi}\sum_{p=1}^{N}\left[C_{\mathrm{nd}}D\frac{\partial g(\kappa|\mathbf{r}_p-\mathbf{r}_d|)}{\partial\mathbf{n}_p} + g(\kappa|\mathbf{r}_p-\mathbf{r}_d|)\right]\frac{\partial G^{\mathrm{KA}}(\mathbf{r}_s,\mathbf{r}_p)}{\partial\mathbf{n}_p}. \tag{13}$$

Equation (13) is an explicit expression of the Green function where the computation time will increase only linearly with the system size. Also, one of the main advantages of Eq. (13) is that the values of $\partial G^{\mathrm{KA}}/\partial\mathbf{n}_p$ given by Eq. (10) need only to be calculated once for all possible source-plane distances $\overline{Z}$ and $\overline{\mathbf{R}}$ values present in the geometry, recalling or interpolating its value each time the source and plane positions $\mathbf{r}_s$ and $\mathbf{r}_p$ hold Eq. (11). This considerably increases the computation speed by reducing the number of Fourier transforms, especially in the cases in which many different source positions need to be generated, such as in DOT. We would like to state that an analogous expression to Eq. (13) can be easily found for diffusive/diffusive interfaces by means of the diffusive/diffusive reflection and transmission coefficients [33].

IV. NUMERICAL RESULTS

In order to study the limits of validity of the KA, we compare the performance of the exact solution, based on Eq. (6), with the approximate solution, based on Eq. (13), using the geometry shown in Fig. 3. The cylinder has a radius R, length h, and is illuminated by an infinite longitudinal light source running parallel to the cylinder at ($R_s = R - l_{\mathrm{tr}}$ $\theta = 0$), where $l_{\mathrm{tr}} = 1/\mu_s'$ is the transport mean free path. The refractive indices inside and outside the diffusive volume are that of water, i.e., $\nu_{\mathrm{in}} = 1.333$, and of air, $\nu_{\mathrm{out}} = 1$, respectively. An angular scan is performed at ($R_d = R - l_{\mathrm{tr}}$, $z = 0$). In order to quantify the accuracy of the approximation, we shall define the error in percentage as

$$(\mathrm{Error}) = 100\times\int_{2\pi}|1 - U^{\mathrm{KA}}(R_d,\theta)/U^{\mathrm{ET}}(R_d,\theta)|\,d\theta, \tag{14}$$

where U^{ET} is the exact solution obtained from the ET [23] using 2D Green functions (corresponding to an infinitely long cylinder), and U^{KA} is the solution obtained from the KA using a 3D geometry (corresponding to a cylinder of length h). In order to solve for the ET by means of Eq. (6) for a cylinder and a line source, we used the corresponding Green function in 2D, $g(\kappa|\mathbf{r}_s-\mathbf{r}_d|) = \pi i H_0^{(1)}(\kappa|\mathbf{r}_s-\mathbf{r}_d|)$, where $H_0^{(1)}$ is the zero-order Hankel function of the first kind.

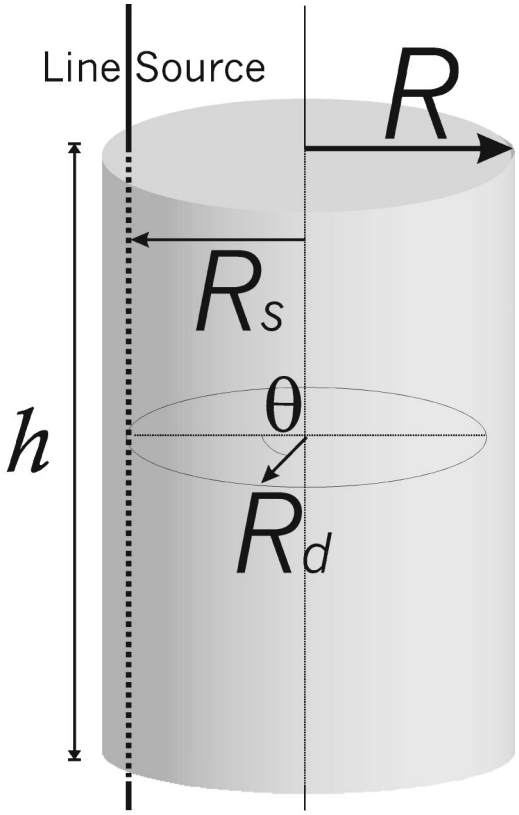

FIG. 3. Geometry used for the study of the limits of validity of the KA.

In all cases, the KA results will be generated for a cylinder of height $h = 10$ cm and no lids, consisting of $N = 9191$ surface discretisation points. The value of h was such that no variation in the results was found by increasing its value. The results generated with the ET in 2D consisted of $N = 360$ points. In these cases, a lookup table consisting of 257 values for $\overline{\mathbf{R}}$ and a maximum value for $\overline{Z}$ of R was generated, with a distance of 0.1 cm between values. We performed the study in the continuous illumination mode (CW), since in this modality light suffers less attenuation. For higher attenuation values the multiple reflections between the surface boundary decays, and, therefore, the limits of validity here found will apply to all frequency modulation values. A similar study was performed for different modulation frequencies, finding the error in amplitude in the order or smaller than in its corresponding CW case, and a difference in phase in the order of 1 to 5 degrees.

In Fig. 4 we show the error committed by the KA for different values of R, absorption, and scattering coefficients as compared to the ET solution. The results shown here are representative of biologically relevant optical properties. On the whole, the approximation works well ($<5\%$ error) for $R > 3L_d$, where $L_d = \sqrt{D/\mu_a}$ is the diffusion length in CW ($\omega = 0$). That is, to maintain an error below 5% for $R = 1.5$ cm, L_d should be larger than 0.5 cm for $\mu_s' = 5\ \mathrm{cm}^{-1}$, which gives $\mu_s' > 0.13\ \mathrm{cm}^{-1}$ (see Fig. 4). When diffusive/

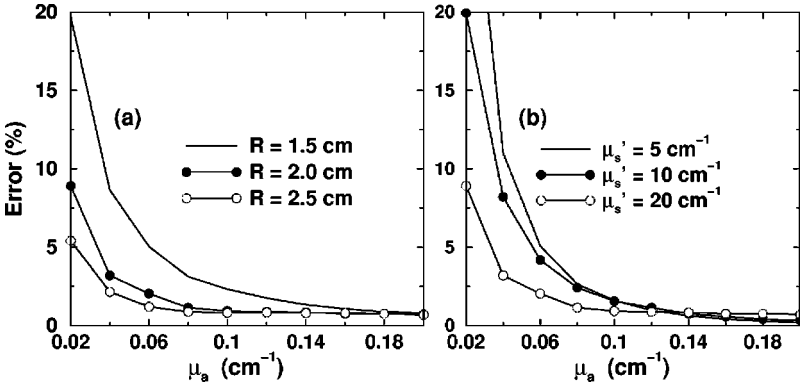

FIG. 4. (a) Error in percentage committed for different values of μ_a and cylinder radii R. In all cases $\mu_s'=10\ \mathrm{cm}^{-1}$. (b) Same as (a) but for different values of μ_s' for $R=1$ cm.

diffusive interfaces are considered the approximation works much better, and is valid for $2R>3L_d$ because lower reflectivity is attained in this case (similar results where obtained in Ref. [31]).

In order to establish the effect of the surface topography, we have studied the same configuration as in Fig. 4, but have added a sine profile of amplitude 0.5 cm and period $\pi/4$ to the surface. In this case, a lookup table consisting of 257 values for $\overline{\mathbf{R}}$ and 76 values for $\overline{Z}$ was generated, with a distance of 0.1 cm between values. The error between the ET and the KA, is now depicted in Fig. 5 for two cases of source position (Fig. 5 top row $R_s=2.3$ cm, bottom row $R_s=1.5$ cm). In addition, we have also represented this error when, instead of the KA, we simply use the homogeneous Green function, Eq. (2), to calculate the source radiation using Eq. (3). Generally, the KA approximation calculates the average intensity with errors that are less than 5% [see Fig. 5(a) and Fig. 5(c)], except in the shadow regions of the corrugations. This *shadowing effect* appears when certain surface areas are blocked from the source by the geometry of the interface. Since these shadow areas are not taken into account in the KA, the KA predicts higher values of the intensity. A first approximation to this problem would be to include a geometry-dependent constant that will assign a zero value to those surface points not visible from the source position. Such a geometry factor was included and the results presented in Fig. 5 repeated, finding no important improvement. Another way of improving the KA is to include second order reflections, but this would render the method time consuming and thus would loose its potential as a fast analytical tool.

In Fig. 5 we also see that the approximation yields errors in the order of 5–10% close to the boundaries, where the Green function has low values due to the boundary conditions that force the average intensity to zero at approximately one extrapolated distance (l_{tr}) from the interface [28]. When the error obtained from the KA is compared with that obtained by using a mere homogeneous Green function [see Fig. 5(b) and Fig. 5(d)], we see that the KA is more accurate by one order of magnitude. Similar figures to those represented in Fig. 5 were generated for a modulation frequency of $\omega=200$ MHz. In this case we found that the error distribution in amplitude was very similar to the cases presented in Fig. 5, with slightly smaller values, and thus results are not shown. This is expected due to the lower reflectivity of the boundaries. The maximum phase difference found for the

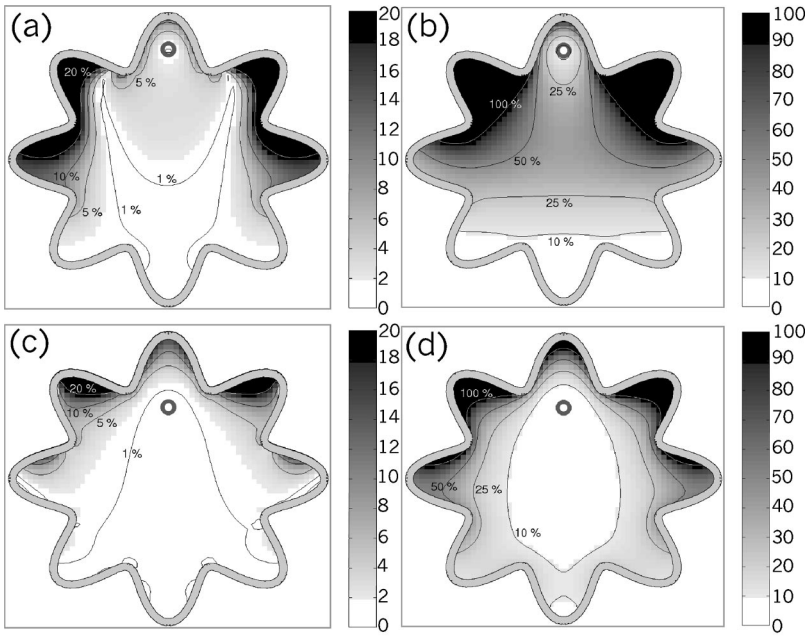

FIG. 5. Error committed in percentage when using the KA [(a) and (c)] and when using the homogeneous Green function [(b) and (d)] for a cylinder of $R=2.5$ cm with a sine profile on the boundary of amplitude 0.5 cm, and period $\pi/4$. The following source locations are considered: ($R_s=2.3$ cm, $\theta=0$) [(a) and (b)]; ($R_s=1.5$ cm, $\theta=0$) [(c) and (d)]. In all cases $\mu_s'=10\ \mathrm{cm}^{-1}$, $\mu_a=0.1\ \mathrm{cm}^{-1}$.

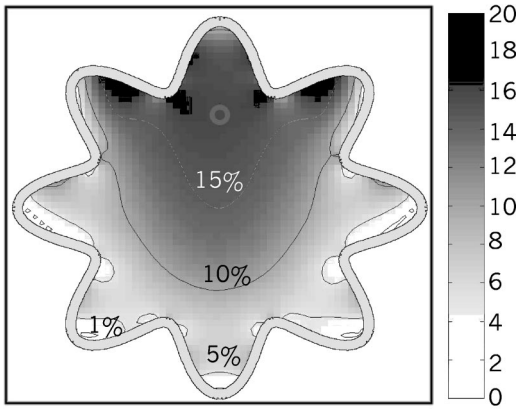

FIG. 6. Error committed in percentage for the scattered Green function [see Eq. (15)] when using the KA for a cylinder of $R=2.5$ cm with a sine profile in the boundary of amplitude 0.5 cm, and period $\pi/4$. Source locations ($R_s=1.5$ cm, $\theta=0$), $\mu_s'=10\ \mathrm{cm}^{-1}$, $\mu_a=0.1\ \mathrm{cm}^{-1}$.

KA was 2 deg at the shadow regions and 1 deg near the boundaries. When compared to the infinite Green function we found 60 deg difference at the shadow regions and a minimum phase difference of 10 deg.

In general terms of the KA, it is expected that lower spatial frequencies **K** (or angles of incidence close to the normal in the electromagnetic case [25,26]) will yield more accurate solutions than high spatial frequencies (or grazing angles of incidence in the electromagnetic case [25,26]). This may be translated to diffusive waves in the following manner. In the cases in which the point source is close to the interface, high spatial frequencies play an important role. It is in these cases in which the KA is expected to fail for diffusive waves, since then multiple reflections are predominant. On the other hand, when the source is far (more than one diffusion length) from the interface, due to high damping the high frequencies components of the incident wave do not contribute significantly to the incident wave at the interface, reducing the multiple reflections. This effect is shown in Fig. 6, where we represent the error when considering the perturbation caused by the interface, i.e., the scattered wave G_{SC} [see Eq. (13)]:

$$G_{\mathrm{SC}}^{\mathrm{KA}}(\mathbf{r}_s,\mathbf{r}_d)=G^{\mathrm{KA}}(\mathbf{r}_s,\mathbf{r}_d)-g(\kappa|\mathbf{r}_s-\mathbf{r}_d|). \qquad (15)$$

As seen in Fig. 6, the error obtained from the KA at long distances from the source where only low values of **K** contribute to the incident field is very low ($<5\%$). On the other hand, values of the scattered wave in the regions where the source is near the interface present larger errors (20%), due to the higher contribution of large values of **K**.

We have tested other values of the period and the amplitude of the sine profile, reaching the same conclusion: outside the shadow regions, and for $R>3L_d$, the error is consistently less than 5%. This also holds true for calculations performed for a rough surface plane, such as in Ref. [34].

As mentioned before, besides its ability to handle arbitrary geometries the KA is attractive due to its computation efficiency. In Fig. 7 we present a comparison of the computation times obtained by using the ET and the KA with a

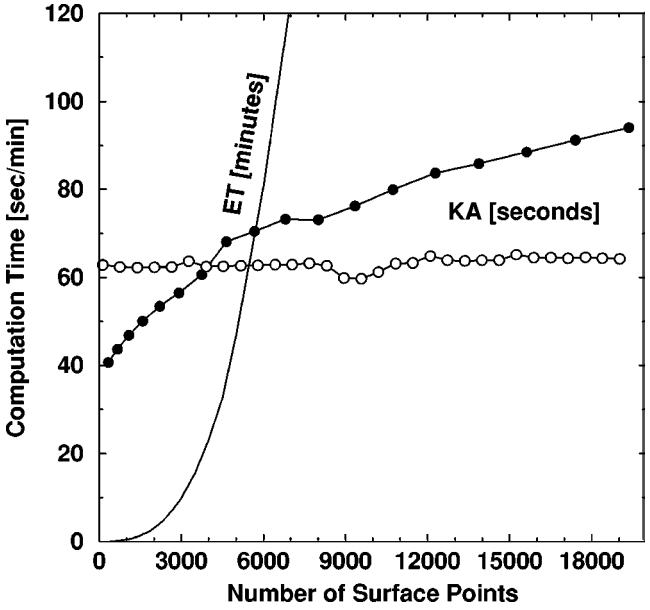

FIG. 7. Computation times for one source-detector pair versus the number of surface points N [see Eq. (13)] for the ET represented in minutes [solid line] and for the KA represented in seconds for the cases: cylinder of radius $R=2$ cm, with its height increased from 0–15 cm [open circles]; and a cylinder with its radius increased from $R=0.5-4$ cm and its height as $h=2R$ [full circles]. Results obtained from a Pentium III running at 650 MHz with 256 Mb memory.

Pentium III running at 650 MHz, with 256 Mb memory. These computation times include the generation of the lookup table for $(\overline{\mathbf{R}},\overline{Z})$ [see Eq. (11)] aforementioned in Sec. III. That is, the computation times presented make use of no *a priori* calculations. In all cases shown here, the lookup table for $(\overline{\mathbf{R}},\overline{Z})$ is generated by finding the range of values $[\min\{\overline{\mathbf{R}}\},\max\{\overline{\mathbf{R}}\}]$ and $[\min\{\overline{Z}\},\max\{\overline{Z}\}]$ present in the geometry, and generating all the corresponding values of Eq. (10), with an increase of one transport mean free path (l_{tr}) between $(\overline{\mathbf{R}},\overline{Z})$ values. This discretisation value can be understood since the diffusion equation in itself has no meaning when considering distances smaller than l_{tr}. Once the lookup table for Eq. (10) is built, the different values present in Eq. (13) are found by interpolation. As mentioned in Sec. III, in order to numerically perform the Fourier transforms 512 **K** values were used for each dimension (i.e., 512×512), with $|d\mathbf{K}|\sim0.123$. The computation times are represented in Fig. 7 versus the number of discretisation points N [see Eqs. (6) and (13)], which in the ET are independent on the dimension and shape of the geometry. In the case of the KA, since the computing time is dependent on the number $(\overline{\mathbf{R}},\overline{Z})$ values, we present two cases: a case in which we have a cylinder of radius $R=2$ cm, and increase its height from 0–15 cm (open circles in Fig. 7); and a cylinder that is increased in radius R from 0.5–4 cm and its height as $h=2R$ (full circles in Fig. 7). In all the KA cases the discretized areas are kept to be $dS=0.1\times0.1\ \mathrm{cm}^2$. Due to the fact that both the KA and the ET perform equivalently for any number of source-detector pairs once the surface values are found, the computation

times presented in Fig. 7 correspond to the forward problem for one source-detector pair. When considering the computational times for the ET in Fig. 7, we see that there is an approximately quadratic increase with respect to N (note the difference in scale between the KA and the ET). On the other hand, when considering the KA, we see that the increase is approximately linear for both cases, the difference in slope due to the dependence on the number of $(\overline{\mathbf{R}},\overline{Z})$ values generated. As a practical example, the number of discretization points for a sphere of radius 2 cm needed in order to maintain a $1l_{\mathrm{tr}}$ distance between points is in the order of 5000. If we compare the speed of the KA and the ET in this case we obtain 70 s and 50 min, respectively, yielding the KA as approximately 40 times faster. A more realistic surface such as the adult head, would imply an equivalent radius of at least 4 cm, and thus $N\sim 20\,000$. In this case, the KA takes in the order of 90 s, whereas the ET takes in the order of 45 h for one only forward solution. In this more realistic case the KA is 1800 times faster.

V. CONCLUSIONS

We have presented an approximate method that solves the 3D diffusion equation in geometries of arbitrary shape and size in a linear fashion. This approximation has been compared to the ET solution of the diffusion equation [23], a boundary-value dependent numerical method that has been extensively used in physical optics due to its high degree of accuracy [25]. We have found that when the average radius of the geometry considered is $R>3(D/\mu_a)^{1/2}$, the method performs with an error less than 5%. Therefore, with the KA we can generate general Green functions that take into account complex geometries, the computation times of this approximation being very fast compared to the rigorous solution, and increasing linearly with the size of the system. The implications of this approximation are several: In the first place, these KA Green functions can be employed in more complex numerical schemes such as the ET [23], so as to reduce the number of discretization points needed to solve the forward problem. As an example, the problem of an object embedded in an arbitrary volume would be reduced to an object on its own by using the KA Green function. In a similar manner, it can be used to improve the reconstruction schemes based on Rytov or Born approximations, such as algebraic reconstruction technique (ART) and simultaneous iterative reconstructive technique (SIRT) [11–15]. Second, since the computation times and the memory requirements increase linearly with the size of the system, the KA may be used to describe light propagation in large volumes such the adult head, the calf, etc. It is in these large volumes where rigorous numerical methods have problems due to the great amount of memory required for matrix inversion, and the need of extremely large computational times to solve the inverse problem. We believe that this approximation will aid to the development of real time diagnostics with diffuse light in the presence of complex boundaries.

ACKNOWLEDGMENTS

J.R. acknowledges a European TMR grant under Project No. FMRX-CT96-. V.N. acknowledges support in part from DRG-1638 of the Cancer Research Fund of the Damon Runyon–Walter Winchell Foundation and the U.S. Army (CDMRP BC995360). V.N. and M.N-V. also acknowledge a TMR contract from the EU. This work has received partial support from the Spanish DGICYT.

[1] A. Yodh and B. Chance, Phys. Today **48**(3), 38 (1995).
[2] S. K. Gayen and R. R. Alfano, Opt. Photonics News **7**, 17 (1996).
[3] E. B. de Haller, J. Biomed. Opt. **1**, 7 (1996).
[4] M. A. Franceschini, K. T. Moesta, S. Fantini, G. Gaida, E. Gratton, H. Jess, W. W. Mantulin, M. Seeber, P. M. Schlag, and M. Kaschke, Proc. Natl. Acad. Sci. U.S.A. **94**, 6468 (1997).
[5] D. Grosenick, H. Wabnitz, H. H. Rinneberg, T. Moesta, and P. M. Schlag, Appl. Opt. **38**, 2927 (1999).
[6] V. Ntziachristos, A. G. Yodh, M. Schnall and B. Chance, Proc. Natl. Acad. Sci. U.S.A. **97**, 2767 (2000).
[7] V. Ntziachristos and B. Chance, Breast Cancer Res. Treat. **3**, 41 (2001).
[8] V. Ntziachristos, X. H. Ma, A. G. Yodh, and B. Chance, Rev. Sci. Instrum. **70**, 193 (1999).
[9] V. Ntziachristos, X. H. Ma, and B. Chance, Rev. Sci. Instrum. **69**, 4221 (1998).
[10] S. R. Arridge, Inverse Probl. **15**, R41 (1999).
[11] A. C. Kak and M. Slaney, *Principles of Computerized Tomographic Imaging* (IEEE, New York, 1988).
[12] M. A. O'Leary, D. A. Boas, B. Chance, and A. G. Yodh, Opt. Lett. **20**, 426 (1995).
[13] D. A. Boas, L. E. Campbell, and A. G. Yodh, Phys. Rev. Lett. **75**, 1855 (1995).
[14] M. A. O'Leary, D. A. Boas, X. D. Li, B. Chance, and A. G. Yodh, Opt. Lett. **21**, 158 (1996).
[15] X. De Li, T. Durduran, A. G. Yodh, B. Chance, and D. N. Pattanayak, Opt. Lett. **22**, 573 (1997).
[16] C. P. Gonatas, M. Ishii, J. S. Leigh, and J. C. Schotland, Phys. Rev. E **52**, 4361 (1995).
[17] S. R. Arridge, Appl. Opt. **34**, 7395 (1995).
[18] H. Jiang, K. D. Paulsen, U. L. Osterberg, B. W. Pogue, and M. S. Patterson, J. Opt. Soc. Am. A **13**, 253 (1996).
[19] J. Chang, H. L. Graber, and R. L. Barbour, IEEE Trans. Biomed. Eng. **44**, 810 (1997).
[20] T. Durduran, J. P. Culver, M. J. Holboke, X. D. Li, L. Zubkov, B. Chance, D. N. Pattanayak, and A. G. Yodh, Opt. Express **4**, 247 (1999).
[21] X. Li, D. N. Pattanayak, T. Durduran, J. P. Culver, B. Chance, and A. G. Yodh, Phys. Rev. E **61**, 4295 (2000).
[22] D. L. Everitt, S. Wei, and X. D. Zhu, Phys. Rev. E **62**, 2924 (2000).
[23] J. Ripoll and M. Nieto-Vesperinas, J. Opt. Soc. Am. A **16**, 1453 (1999).

[24] R. Aronson, J. Opt. Soc. Am A **116**, 61 (1999).
[25] P. Beckmann, Prog. Opt. **61**, 55 (1961).
[26] J. M. Soto-Crespo and M. Nieto-Vesperinas, J. Opt. Soc. Am. A **6**, 367 (1989).
[27] M. Nieto-Vesperinas, *Scattering and Diffraction in Physical Optics* (Pergamon, New York, 1996).
[28] R. Aronson, J. Opt. Soc. Am. A **12**, 2532 (1995).
[29] N. G. Chen and J. Bai, Phys. Rev. Lett. **80**, 5321 (1998).
[30] G. Popescu, C. Mujat, and A. Dogariu, Phys. Rev. E **61**, 4523 (2000).
[31] J. Ripoll, V. Ntziachristos, J. P. Culver, D. N. Pattanayak, A. G. Yodh, and M. Nieto-Vesperinas, J. Opt. Soc. Am. A **18**, 821 (2001).
[32] J. Ripoll, M. Nieto-Vesperinas, and R. Carminati, J. Opt. Soc. Am. A **16**, 1466 (1999).
[33] J. Ripoll and M. Nieto-Vesperinas, Opt. Lett. **24**, 796 (1999).
[34] J. Ripoll and M. Nieto-Vesperinas, J. Opt. Soc. Am. A **16**, 1947 (1999).